Title
X-Ray Spectroscopic Characterization of BaO, Ba(OH)2, BaCO3, and Ba(NO3)2

Authors
Karslıoğlu, Osman
Trotochaud, Lena
Zegkinoglou, Ioannis
et al.

Publication Date
2018-05-01

DOI
10.1016/j.elspec.2018.03.008

Peer reviewed

X-Ray Spectroscopic Characterization of BaO, $Ba(OH)_2$, $BaCO_3$, and $Ba(NO_3)_2$

Osman Karslıoğlu,[1] Lena Trotochaud,[1] Ioannis Zegkinoglou,[1,†] and Hendrik Bluhm[1,2,*]

[1] Chemical Sciences Division, Lawrence Berkeley National Laboratory, Berkeley, CA, 94720 USA
[2] Advanced Light Source, Lawrence Berkeley National Laboratory, Berkeley, CA, 94720 USA
† Present address: Department of Physics, Ruhr University Bochum, 44780 Bochum, Germany
* Corresponding author (hbluhm@lbl.gov)

ABSTRACT

Simple inorganic barium compounds are difficult to study spectroscopically in the surface sensitive soft X-ray regime due to significant surface contamination that can dominate the spectra. Here we present a near-edge X-ray absorption (NEXAFS) and X-ray photoelectron spectroscopic (XPS) study of four barium compounds: BaO, $Ba(OH)_2$, $BaCO_3$, and $Ba(NO_3)_2$. Using an ambient-pressure XPS instrument we prepared thin film samples in situ, which provided a high degree of control over the surface chemistry and significantly reduced the amount of contamination. The O K-edge spectrum for BaO presented here is in excellent agreement with the latest calculations in the literature, and indicates that experimental spectra in the literature for this compound may have suffered from carbonate contamination.

Keywords: NEXAFS; APXPS; barium oxide; barium hydroxide; barium carbonate; barium nitrate

1 Introduction

Barium is a constituent of many compounds used in technological applications such as NO_x traps for automotive exhaust abatement systems **(Takahashi et al. 1996)**, UHV getters **(Cooper 1929, Lederer 1934)**, solid oxide fuel cell electrodes **(Yang et al. 2011, Li et al. 2012)**, second-harmonic generation crystals in non-linear optics **(Miller et al. 1963)**, and high-temperature superconductors **(Wu et al. 1987)**.

NO_X traps are part of the abatement technology called "NO_X storage and reduction" (NSR), which is used in combination with lean-burn engines, i.e. engines where the O_2 content is higher than stoichiometric, such as diesel and some gasoline engines. In this technology, $BaO/BaCO_3$ is used as a NO_x (NO and NO_2) trap by forming $Ba(NO_3)_2$ to store the NO_x which is formed during the combustion process. $Ba(NO_3)_2$ is then decomposed during a relatively short period where NO_x is released and reacted with hydrocarbons on precious-metal catalysts to regenerate the storage material.

The study of complex, multicomponent systems with core-level spectroscopy techniques **(Kim et al. 2006, Kim et al. 2008, Kim et al. 2009)**, such as ambient pressure X-ray photoelectron spectroscopy (APXPS) and X-ray absorption spectroscopy/spectromicroscopy, often requires that reliable reference data are available. In particular, NEXAFS is often used to characterize heterogeneous catalytic reactions under in situ conditions. The correct interpretation of in situ NEXAFS data is greatly aided by knowledge of the spectra of the pure components that one can expect under reaction conditions; in the case of an NSR catalyst, these components are BaO, $BaCO_3$, $Ba(NO_3)_2$, and $Ba(OH)_2$.

Elemental Ba is an extremely reactive metal even at room temperature, especially towards oxygen and halogens **(Boffito 2000)**. BaO forms hydroxides and carbonates with H_2O and CO_2 in air. It is thus difficult to avoid contamination of the pure materials which might lead to erroneous interpretations of spectral fingerprints of this compound. $Ba(OH)_2$ has been previously investigated by hard X-ray absorption spectroscopy at the Ba L-edge **(Finch et al. 2010)**, but no soft X-ray studies have been reported to date, and neither has a NEXAFS characterization of $Ba(NO_3)_2$.

We here present an in situ spectroscopy approach to identify the spectral fingerprints of four compounds of Ba, namely BaO, $Ba(OH)_2$, $BaCO_3$, and $Ba(NO_3)_2$. By combining NEXAFS and XPS with in situ sample preparation, using the appropriate temperature and gas phase partial pressure, we were able to control the sample chemistry and avoid the presence of impurities. We found the experimental BaO spectrum to be fully consistent with the latest simulations in the literature **(McLeod et al. 2010)**, in contrast to previously reported experimental spectra of BaO **(Nakai et al. 1987, McLeod et al. 2010)**, which show significant levels of carbonate content.

2 Experimental Details

The experiments were performed at the APXPS endstation **(Ogletree et al. 2009)** of the 11.0.2 beamline **(Bluhm et al. 2006)** of the Advanced Light Source at Lawrence Berkeley National Laboratory. The angles between the surface normal and the incident beam, the polarization vector, and the analyzer axis were 25°, 65.5°, and 40°, respectively.

BaO layers (10–20 nm) were deposited on a Pt(111) substrate by electron-beam evaporation of BaO powder (Sigma-Aldrich, 99.99 % metals basis). An evaporator (Mantis QUAD-EV-C) with an Al_2O_3-lined Ta crucible was used. The Pt crystal was free of impurities except for small quantities of carbon. Before the preparation of a new compound, the crystal was cleaned in HCl solution (pH ~0) to remove the previously deposited barium compound and afterwards rinsed with ultrapure water. The sample was mounted on a ceramic button heater (Heatwave Labs) using stainless steel (SS-304) clips. A K-type thermocouple was spot-welded onto the side of the crystal. The Pt sample was heated to > 900 °C before BaO deposition. Small quantities of carbon contaminants on the Pt surface remained buried under the relatively thick BaO layers, and did not show up later in the spectra. The resulting BaO films, which initially also included carbonate and hydroxide species, were treated in situ to obtain the pure oxide. The details of each preparation are given in the Results section. After the in situ treatments, all layers were sufficiently thick to attenuate the Pt signal from the substrate almost completely at an electron kinetic energy (KE) of 800 eV (IMFP ~ 1.9 nm).

As a water vapor source, we used ultrapure (18.2 MΩ cm) H_2O degassed via freeze–pump–thaw cycles. NO_2 and CO_2 (> 99.99 %) were used without further purification. All gases, including water vapor, were introduced to the chamber via variable precision leak valves.

NEXAFS spectra were collected in the partial electron yield (PEY) mode by using the APXPS analyzer as partial electron yield detector. For each spectrum, a KE window with a width of ~20 eV was chosen such that no photoemission peak moved through the KE window during the NEXAFS scan.

Binding energy calibration for each photon energy (PE) was done by using the Fermi edge of the Pt substrate before BaO deposition. The reproducibility of PEs was checked before the experiment and found to be better than 0.1 eV. PE calibration was performed for the NEXAFS measurements (single point) at the high PE end of the spectra by using the second order light from the monochromator. An intense photoelectron peak from the sample was measured using both PEs, with the difference of the peak positions in KE giving the exact PE. The accuracy of the PE scales was thus determined to be better than 0.1 eV. Both for XPS and NEXAFS, the spectral resolution was not limited by the electron analyzer or the beamline, but rather by the intrinsic Gaussian broadening. NEXAFS background correction was applied by dividing the spectrum from the sample by the spectrum from clean Pt(111), which was acquired just before BaO deposition. The same PE calibration was also applied to the background spectrum from Pt.

3 Results and Discussion

In the next four sections, we present the XPS and NEXAFS spectra for BaO, $Ba(OH)_2$, $BaCO_3$, and $Ba(NO_3)_2$. After these, we discuss the implications of the results here for the published data in the literature. Before moving on to the results, we summarize the core level binding energies determined from XPS for BaO, $Ba(OH)_2$, $BaCO_3$, and $Ba(NO_3)_2$ in Table 1.

Table 1 Core level binding energies for BaO, $Ba(OH)_2$, $BaCO_3$, and $Ba(NO_3)_2$

		BE (eV)	FWHM (eV)
BaO	O 1s	527.8	1.2
	Ba 4d	88.8 / 91.4	1.6
$Ba(OH)_2$	O 1s	530.8	1.3
	Ba 4d	90.0 / 92.6	1.3
$BaCO_3$	O 1s	531.7	1.6
	Ba 4d	90.1 / 92.7	1.7
	C 1s	289.9	1.3
$Ba(NO_3)_2$	O 1s	533.6	1.3
	Ba 4d	91.0 / 93.6	1.4
	N 1s	407.9	1.1

3.1 BaO

NEXAFS and XPS spectra of BaO were collected while the sample was held at 540 °C under 1×10^{-5} Torr O_2 to prevent contamination by CO_2 and H_2O from the chamber residual background pressure and X-ray induced chemical reduction. The XPS spectra in the O 1s, Ba 4d, and C 1s regions for a 20 nm thick BaO layer are shown in Figure 1. The photon energies are 735 eV, 300 eV, and 490 eV, respectively. The main O 1s signal is a symmetric peak at 527.8 eV, in agreement with the literature **(Verhoeven and Van Doveren 1980, Mudiyanselage et al. 2009)**. The small peak in the O 1s region at ~532 eV is due to the formation of $BaCO_3$ from the residual CO_2 in the chamber. The C 1s signal due to carbonate formation is small, but visible in the C 1s spectrum at ~289 eV. Ba 4d peaks are at 88.8 eV and 91.4 eV for the 5/2 and 3/2 spin-orbit components, respectively. A broad satellite is observed between 95–103 eV, which is probably due to the main energy loss feature of bulk BaO; it sits ~9.1 eV away from the main peaks, and can be fitted with a Gaussian doublet with ~3.2 eV FWHM. The electron energy loss spectrum of BaO from the literature indeed shows a broad feature between 8–10 eV **(Protheroe et al. 1983)**.

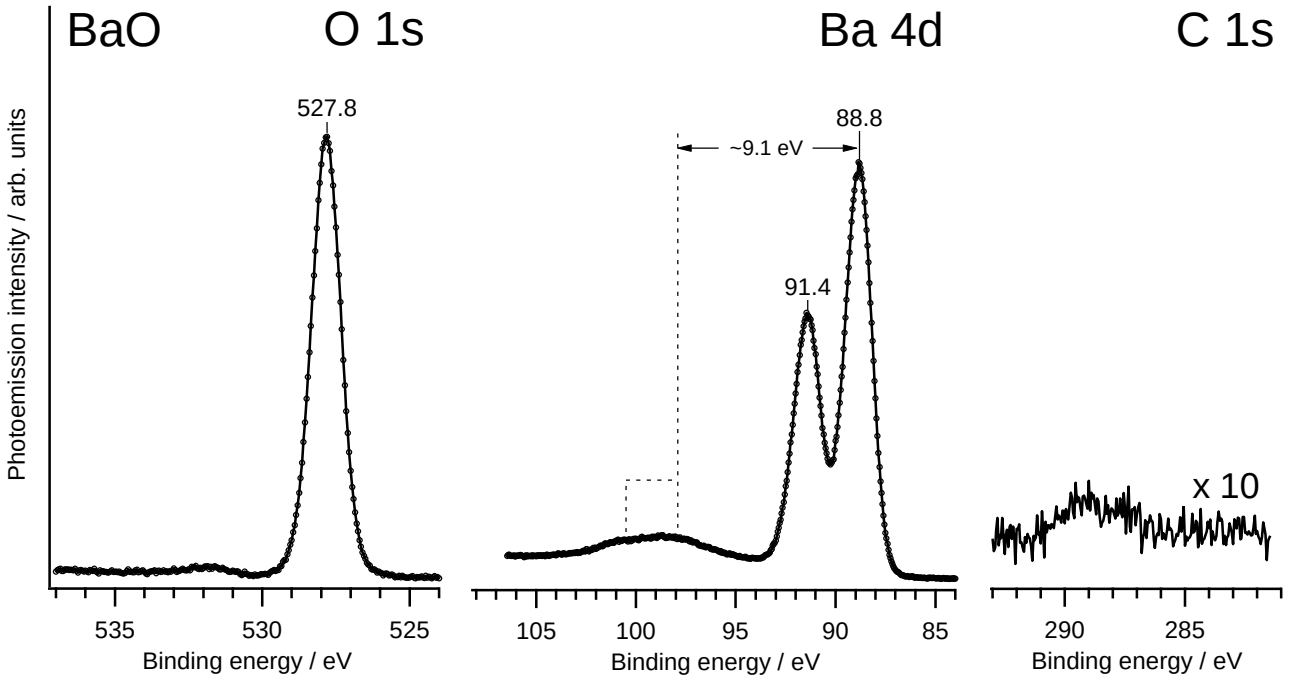

Figure 1 XPS spectra from BaO in the O 1s, Ba 4d, and C 1s regions. Photon energies are 735 eV, 300 eV, and 490 eV, respectively.

The O K-edge NEXAFS spectrum from the same 20 nm thick BaO layer is shown in Figure 2. The electron KE for the PEY detection was 385 eV. The main pre-edge peak is at 531.2 eV, whereas the other most intense peaks are at 534.6 eV, 536.5 eV, 540.4 eV, and 548.2 eV.

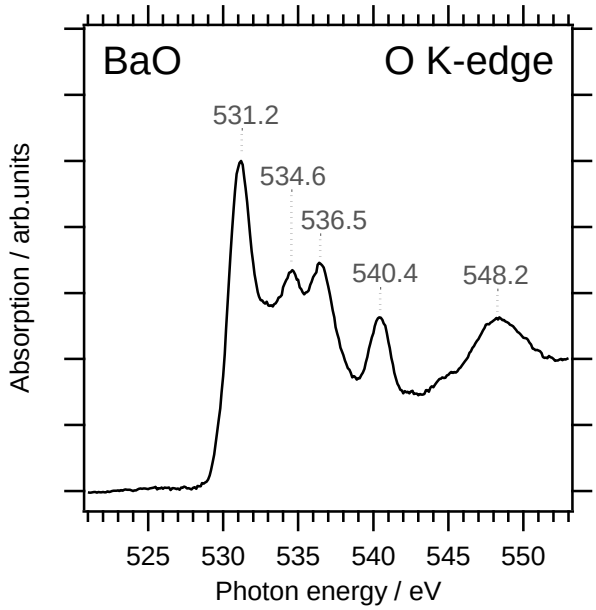

Figure 2 O K-edge NEXAFS spectrum for BaO.

3.2 $Ba(OH)_2$

$Ba(OH)_2$ was prepared by exposing BaO layers to H_2O vapor. The sample preparation procedures for XPS and NEXAFS measurements were different. XPS spectra were obtained on an ultrathin (~1.2 nm, estimated from the O 1s signal of BaO before and after hydroxylation) layer of $Ba(OH)_2$ without fully hydroxylating the BaO layer, because further exposure to H_2O led to significant carbonate contamination. In contrast, NEXAFS measurements were acquired on a $Ba(OH)_2$ layer that had some carbonate contamination, but was relatively thick (~2.4 nm or thicker). A thicker layer ensured that the PEY NEXAFS signal did not contain any BaO signature, and that the large $Ba(OH)_2$ signal dominated over the small carbonate contamination.

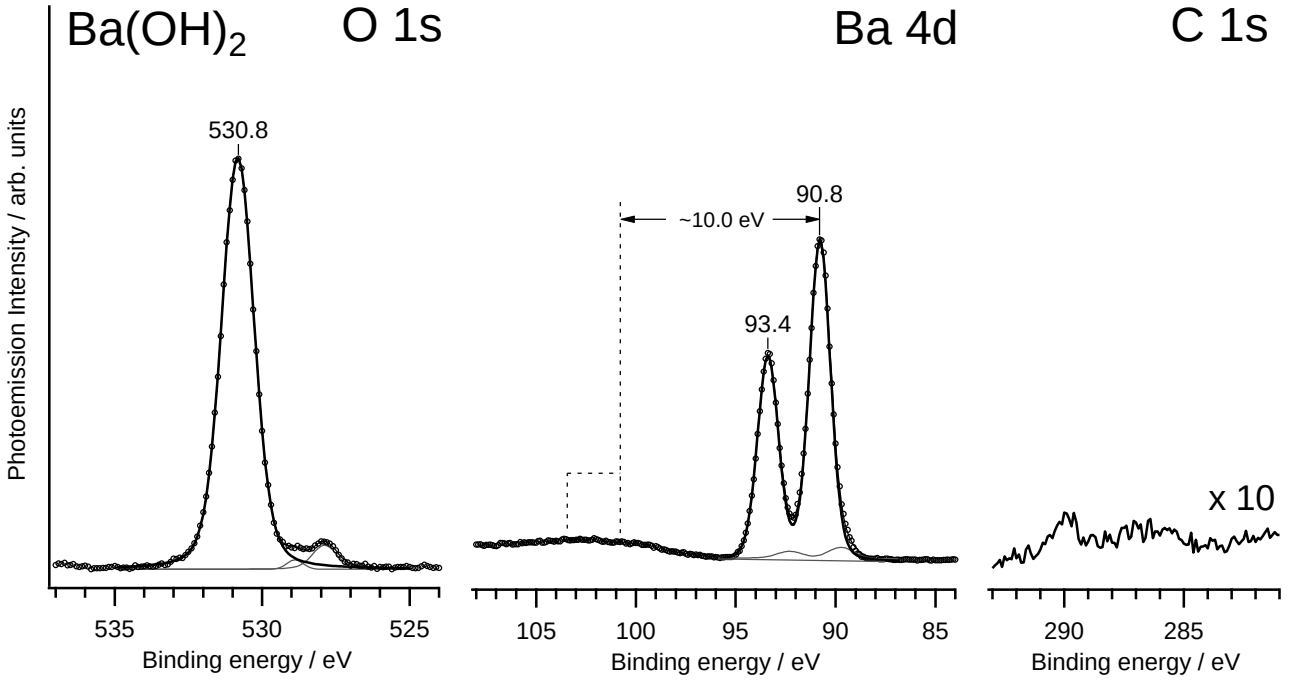

Figure 3 XPS spectra of $Ba(OH)_2$ in the O 1s, Ba 4d and C 1s regions, acquired using photon energies of 735 eV, 320 eV, and 490 eV respectively. The gray lines show the secondary fit components: BaO for O 1s (527.8 eV) and Ba 4d (88.8/91.4 eV); and possibly a BaO–$Ba(OH)_2$ interface component for O 1s (528.9 eV).

O 1s, Ba 4d, and C 1s spectra from $Ba(OH)_2$ are shown in Figure 3. The photon energies are 735 eV, 320 eV, and 490 eV, respectively. $Ba(OH)_2$ was prepared by exposing a BaO layer to 1×10^{-8} Torr H_2O at 490 °C and cooling it to room temperature in H_2O. The spectra were acquired while the sample was still exposed to H_2O. Main peaks are shown with black lines whereas secondary components are marked with light gray lines. Some BaO intensity remains in both the O 1s and Ba 4d regions, indicating that the conversion from oxide to hydroxide is incomplete at the XPS probing depth. The O 1s spectrum shows a small signal between BaO and $Ba(OH)_2$, which might be from the interface between BaO and $Ba(OH)_2$. The main O 1s peak for $Ba(OH)_2$ is at 530.8 eV, 0.2–0.5 eV lower than what was reported in the literature **(Verhoeven and Van Doveren 1982, Tsami et al. 2006, Mudiyanselage et al. 2009)**. Ba 4d peaks for $Ba(OH)_2$ are at 90.0 eV and 92.6 eV for the 5/2 and 3/2 spin-orbit components, respectively.

The main energy loss feature in the Ba 4d spectrum is ~2 times broader (FWHM ≈ 6.0 eV) than that of BaO and can be fitted with a doublet ~10.0 eV away from the main peaks.

The preparation process of the layer that was used for the NEXAFS spectrum of $Ba(OH)_2$ is shown in Figure 4. At each step, we recorded an O K-edge NEXAFS spectrum—sometimes two, to check for beam damage—together with O 1s and C 1s XPS spectra (PE= 735 eV and 490 eV, respectively). After cooling down the BaO layer to room temperature and hydroxylating it by exposure to 5 Langmuir of H_2O, the NEXAFS spectrum still has a component from BaO, clearly seen as the shoulder at ~531 eV. The corresponding C 1s XPS spectrum shows that the layer has a small carbonate contamination. Heating this layer stepwise to 73 °C and 127 °C results in a more intense BaO NEXAFS signal, which disappears when the layer is exposed to 1×10^{-4} Torr H_2O at 127 °C. Further exposure to 5×10^{-2} Torr H_2O results in more carbonate contamination, which shows up in NEXAFS as the peak at ~533 eV as well as in the C 1s XPS spectrum. The layer which was produced by exposure to 1×10^{-4} Torr H_2O at 127 °C shows negligible BaO and $BaCO_3$ signal, and therefore is used as the representative sample for $Ba(OH)_2$ NEXAFS.

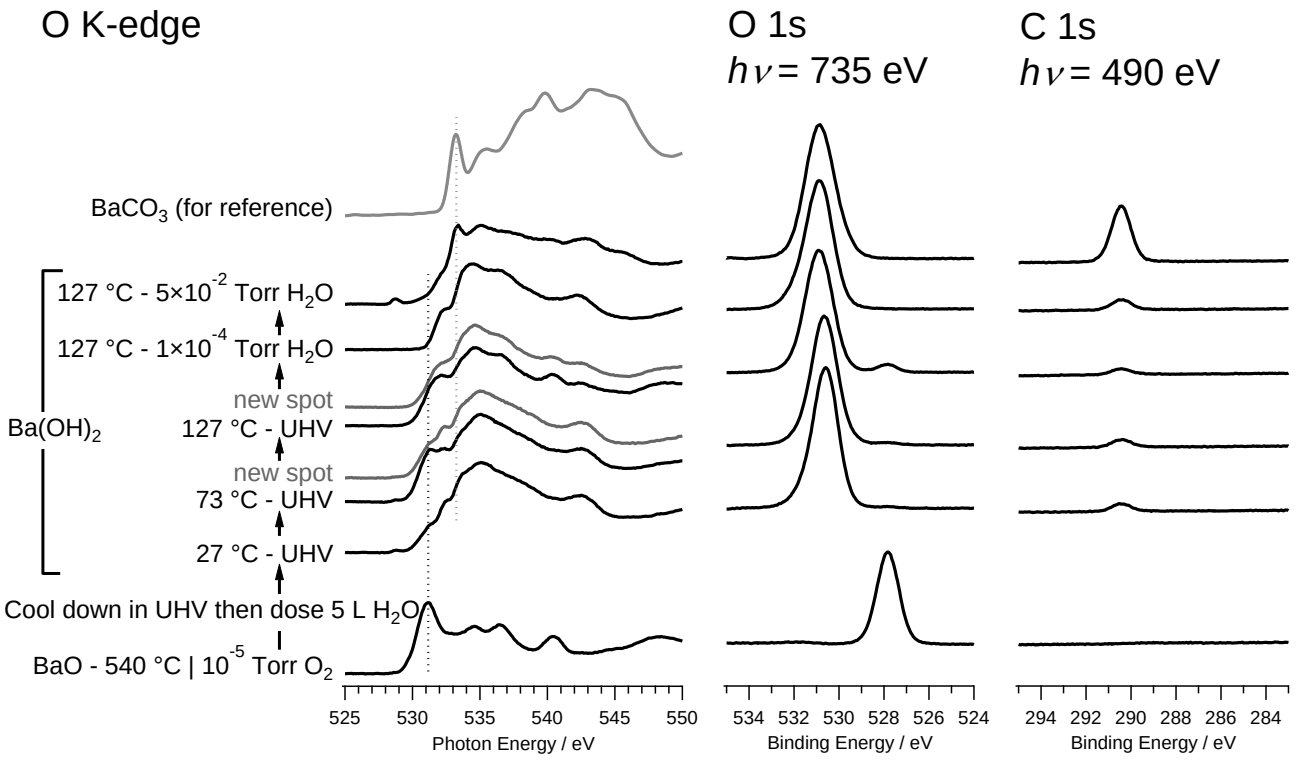

Figure 4 O K-edge NEXAFS, O 1s XPS and C 1s XPS spectra taken during the preparation of $Ba(OH)_2$. Each NEXAFS spectrum (except gray ones) has corresponding O 1s and C 1s spectra, showing the extent of hydroxylation and carbonate contamination. $BaCO_3$ NEXAFS spectrum from a different experiment is also shown for reference.

Figure 5 shows the NEXAFS spectrum of $Ba(OH)_2$ at the O K-edge. The electron kinetic energy for PEY is 385 eV. The first pre-edge feature appears as a shoulder and its peak position is at 532.1 eV. Other distinguishable peaks are at 534.4 eV, 536.5 eV, and 542.2 eV.

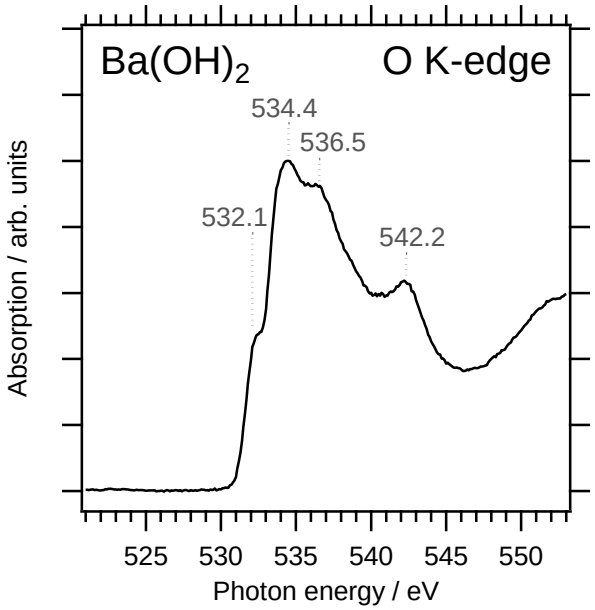

Figure 5 O K-edge NEXAFS spectrum for $Ba(OH)_2$.

3.3 $BaCO_3$

$BaCO_3$ is formed by exposing BaO to 1×10^{-5} Torr CO_2 at 450 °C, and both NEXAFS and XPS spectra are acquired under these conditions. The $BaCO_3$ layer is at least 3.5 nm thick as calculated from the attenuation of the BaO O 1s signal. C 1s, O 1s, and Ba 4d spectra from $BaCO_3$ are shown in Figure 6. All spectra are recorded with a photon energy of 735 eV. The main C 1s peak is at 289.9 eV, whereas the main O 1s peak is at 531.7 eV, both slightly higher (~0.2 eV) binding energies than reported in the literature **(Mudiyanselage et al. 2009)**. Ba 4d peaks are at 90.1 eV and 92.7 eV for the 5/2 and 3/2 spin-orbit components, respectively. The main loss feature is ~10.0 eV away from the main peaks, with a FWHM of ~5.0 eV.

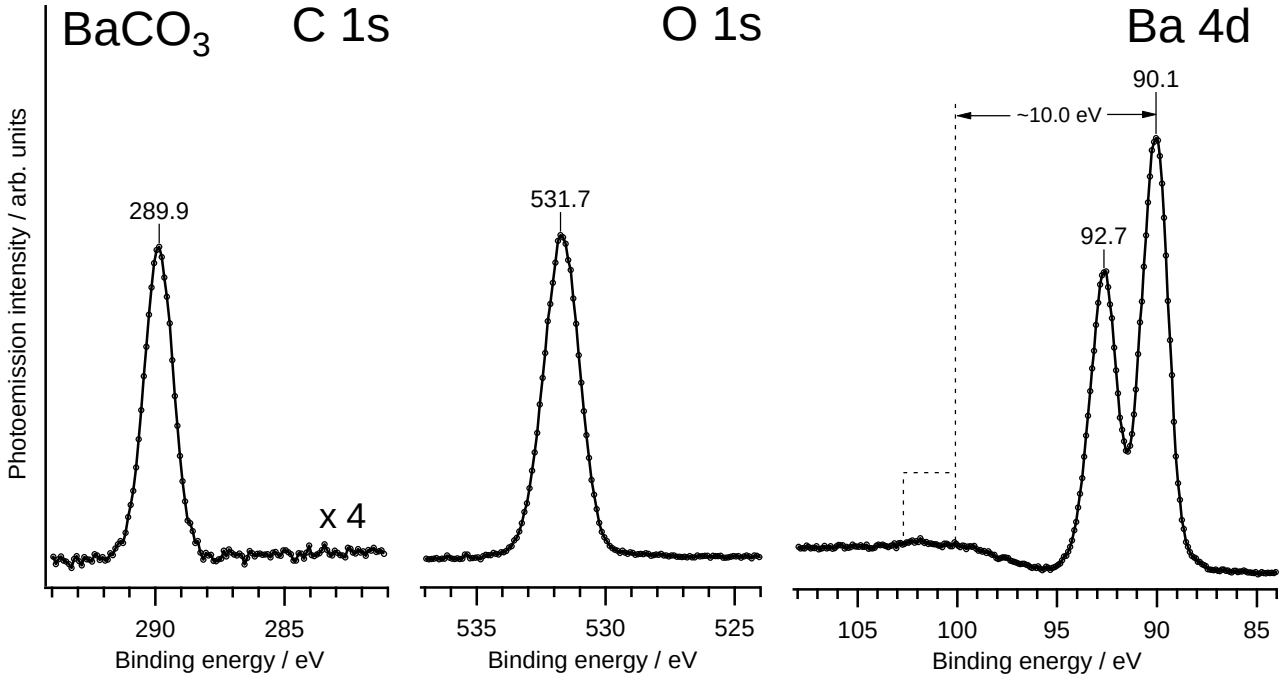

Figure 6 XPS spectra for $BaCO_3$ in C 1s, O 1s, and Ba 4d regions. All spectra are measured using 735 eV photon energy, from a ≥3.5 nm thick $BaCO_3$ layer at 450 °C in 1×10^{-5} Torr CO_2.

NEXAFS spectra for $BaCO_3$ at the O and C K-edges are shown in Figure 7. The electron kinetic energies for PEY are 225 eV and 385 eV for C and O K-edges, respectively. The C K-edge has a sharp pre-edge peak at 290.4 eV, with broader features at 293.9 eV, 300.4 eV, and 302.5 eV. As was observed for many other bulk carbonates **(Garvie et al. 1994, Carrier et al. 1999, Doyle et al. 1999, Zhou et al. 2008)**, the peak at 290.4 eV corresponds to a $\pi^*(a_1' \rightarrow a_2'')$ and the peak at 302.5 eV correspond to a σ^* resonance ($a_1' \rightarrow e'$) that originate from the carbonate ion with an assumed D_{3h} local symmetry **(Ricken et al. 1991)**. The peak at 300.4 eV is likely to be from a different σ^* resonance, for which the D_{3h} symmetry is broken—such as at the surface. C_{3v} and C_{2v} symmetries would indeed lead to another—previously forbidden—σ^* ($a_1 \rightarrow a_1$) resonance. In the case of C_{2v}, a splitting of the e' level to $a_1 + b_2$ takes place and this may give rise to an additional peak or asymmetry. The feature around 293.9 eV is likely the onset of ionization. The O K-edge shows more features than the C K-edge. The relative positions and intensities of the peaks at 533.2 eV, 543.2 eV, and 545.3 eV suggest that they correspond to transitions

to the same levels involved in the π^* and σ^* resonances at the C K-edge. Other notable peaks are at 535.5 eV, 538.3 eV, and 539.8 eV.

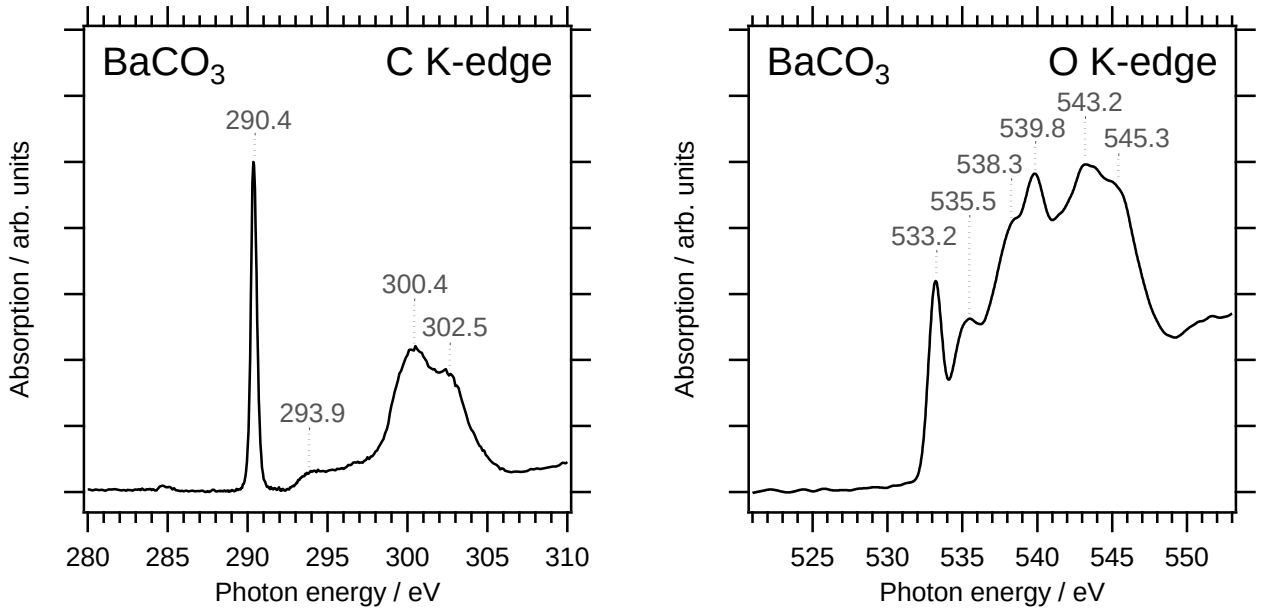

Figure 7 C and O K-edge NEXAFS spectra for $BaCO_3$.

3.4 $Ba(NO_3)_2$

$Ba(NO_3)_2$ was prepared by exposing a >20 nm thick BaO layer to 0.02 Torr NO_2 at room temperature. The $Ba(NO_3)_2$ layer thickness is estimated to be ~3 nm, based on the attenuation of the BaO O 1s signal. All NEXAFS and XPS spectra were taken under 0.02 Torr NO_2 exposure. XPS spectra for $Ba(NO_3)_2$ are shown in Figure 8. The photon energies are 600 eV, 735 eV, 300 eV, and 490 eV for N 1s, O 1s, Ba 4d, and C 1s, respectively. The binding energies of the measured core levels right after dosing (not shown) are ~0.5 eV higher than the presented spectra. This shifting of the peaks starts after ~10 minutes of NO_2 exposure. We interpret this as a change in the work function of the analyzer—due to the reaction of NO_2 with the interior surfaces of the electron energy analyzer—and use the 0.5 eV difference to correct the binding energy scale. However, the binding energies are still not as reliable as the ones we report above for the other Ba compounds, and thus a $\pm$ 0.1 eV uncertainty is indicated.

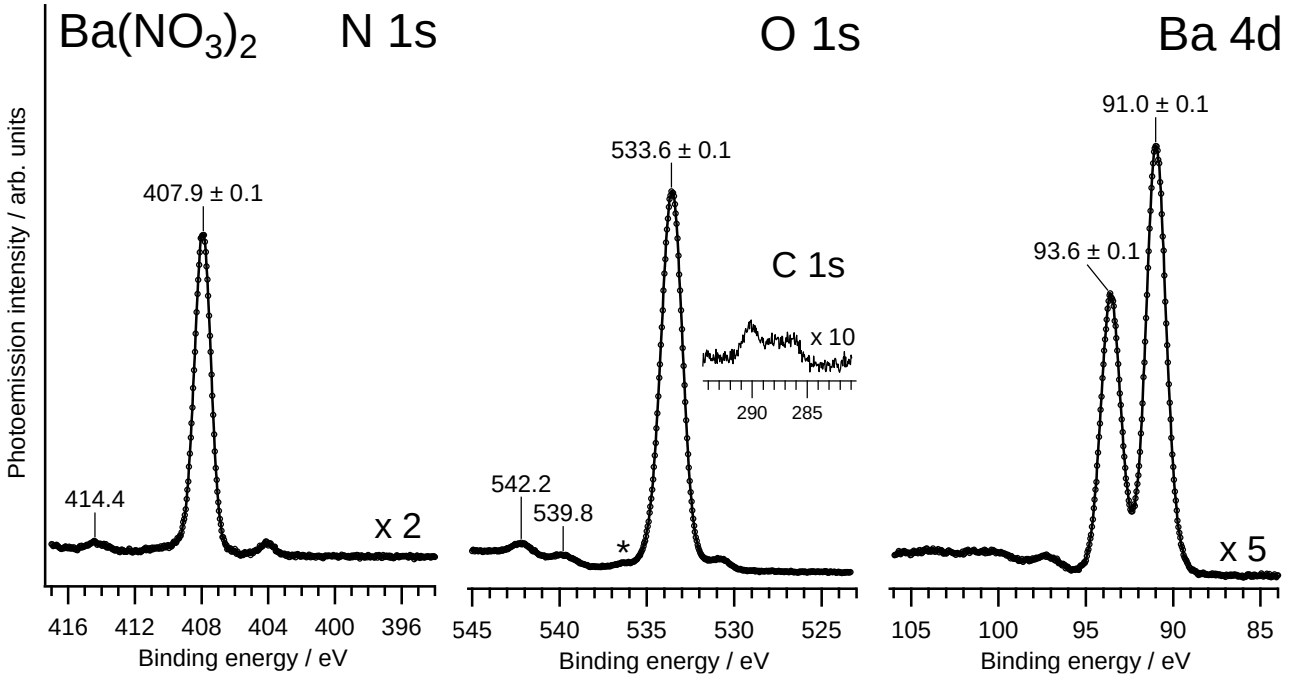

Figure 8 N 1s, O 1s, C 1s, and Ba 4d spectra from a $Ba(NO_3)_2$ layer, measured using photon energies of 600 eV, 735 eV, 490 eV, and 300 eV, respectively. The spectra are recorded with the sample exposed to 0.02 Torr NO_2. The shoulder marked with (*) is the signal from the NO_2 gas.

In addition to the main photoemission peaks, which are in good agreement with the literature **(Schmitz and Baird 2002, Tsami et al. 2006, Mudiyanselage et al. 2009)**, we observe satellite features at ~6 eV higher binding energies in all spectra. These satellites are consistent with the energy loss process that is due to a $\pi \rightarrow \pi^*$ electronic transition in the NO_3^- ion **(McEwen 1961, Yamashita and Kato 1970, Bandis et al. 1999)**. The N 1s spectrum also shows a small peak at ~404 eV which is due to nitrite (NO_2^-) ions. The C 1s spectrum indicates that a small amount of carbon contamination (CO_3^{2-}, C–O, C=O) is present. The O 1s spectrum has a small peak at ~531 eV, which is mostly due to hydroxides (BE = 530.8 eV) but can also originate partly from carbon-containing impurities. The assignment of the peak at ~542 eV is more ambiguous; it is 8.6 eV away from the main peak and might be a loss feature

due to ligand-to-metal charge transfer (i.e. from NO_3^- to Ba^{2+}). Similar transitions observed in alkali (Li, Na, K, Rb, Cs) nitrates are in the range of ~10 eV **(Yamashita and Kato 1970)**, but it is expected to be at a lower energy for Ba^{2+} because its unoccupied orbitals lie at lower energies than those of alkali metal ions. Ba 4d peaks for $Ba(NO_3)_2$ are at 91.0 eV and 93.6 eV for the 5/2 and 3/2 spin-orbit components, respectively.

N and O K-edge NEXAFS spectra of $Ba(NO_3)_2$ are shown in Figure 9. The electron KEs for PEY are 180 eV and 200 eV for N and O edges, respectively. The peak at 405.4 eV originates from nitrate (NO_3^-) ions whereas the small one at 401.7 eV from nitrite (NO_2^-) ions. The presence of nitrites is either due to decomposition of the nitrates under the X-ray beam or the incomplete transformation of BaO to $Ba(NO_3)_2$.

The N and O K-edge spectra are very similar to the spectra of various nitrates reported in the literature **(Rodriguez et al. 2000, Rodriguez et al. 2000, Rodriguez et al. 2001)** and mainly consist of excitations to the unoccupied molecular orbitals of the NO_3^- ion. NO_3^- is isoelectronic with CO_3^{2-} and has the same trigonal planar structure. Thus, analogous to the carbonate ion, the peaks at 405.4 eV and 532.0 eV should originate from the π^* resonance, and the peaks at 415.6 eV and 542.8 eV are likely due to the σ^* resonance. Similar to the CO_3^{2-} case, an additional peak ($a_1 \rightarrow a_1$) for NO_3^- is expected in case of symmetry breaking—at the surface or otherwise—to C_{3v} or C_{2v} **(Rodriguez 1990)**. The peak at 412.0 eV can be due to one of these transitions. It can also be due to one of the σ^* resonances ($a_1 \rightarrow a_1$ or b_2) of NO_2^-. It is 10.3 eV away from the π^* resonance of NO_2^-, which is close to the 9.8 eV difference predicted by Rodriguez **(Rodriguez 1990)**.

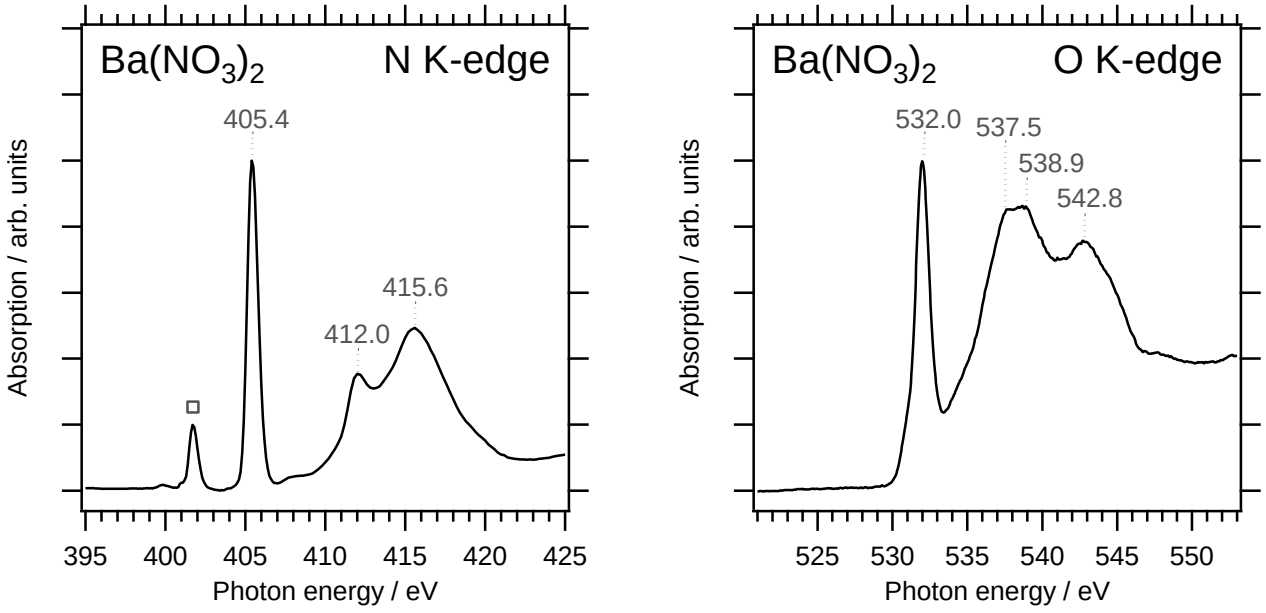

Figure 9 N and O K-edge NEXAFS spectra for $Ba(NO_3)_2$. Nitrite contribution to the N K-edge spectrum is indicated with (☐).

3.5 Discussion

A comparison of experimental O K-edge NEXAFS spectra of BaO from this study and from the literature **(Nakai et al. 1987, McLeod et al. 2010)** is shown in Figure 10. The figure also shows the spectrum of $BaCO_3$ for comparison. The two spectra reported for BaO so far in the literature very much resemble our measurements for $BaCO_3$. The first pre-edge peaks for BaO reported in the literature are ~2.5 eV higher in energy than in our measurements. Assuming the photon energy is reasonably calibrated, such a difference is difficult to explain. In addition, the shape of the NEXAFS spectra from the literature agree much better with our $BaCO_3$ spectrum than with our BaO spectrum.

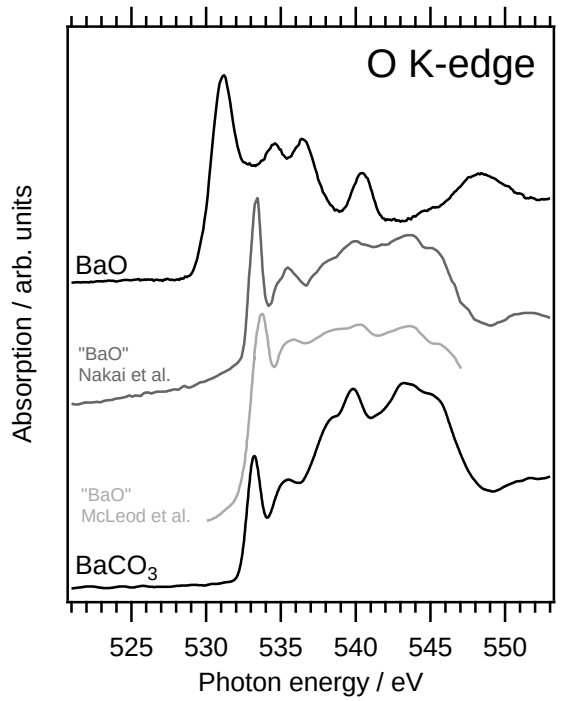

Figure 10 Experimental O K-edge NEXAFS spectra for $BaCO_3$ and BaO (this study, and two from the literature **(Nakai et al. 1987, McLeod et al. 2010)**).

Based on these observations, we conclude that the O K-edge spectra reported so far in the literature are dominated by the signature of $BaCO_3$. It is well-known that alkaline earth metal oxides react with CO_2 from the atmosphere to form carbonates. This may have caused the formation of carbonate in the work of Nakai et al., where powder BaO is used without further treatment. Using total electron yield (TEY), which is a relatively surface sensitive mode, for signal detection may have further exacerbated the carbonate signal. In the work by McLeod et al., it was assumed that the $BaCO_3$ layer was sufficiently thin for the fluorescence-yield (FY) detection mode (which is relatively bulk sensitive) to reduce the contribution of the carbonate layer; nevertheless, the spectral shape in that work also strongly indicates a majority carbonate contribution.

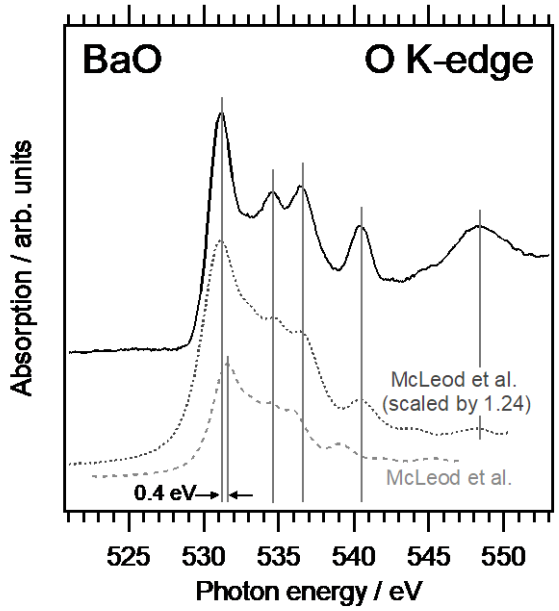

Figure 11 Comparison of the O K-edge NEXAFS spectra from this work (experimental) and from the literature (calculated) **(McLeod et al. 2010)**

Figure 11 shows the measured O K-edge NEXAFS spectrum of BaO together with calculations from the literature **(McLeod et al. 2010)**. The qualitative agreement between the experiment and theory is excellent. The energy difference between the first peaks is 0.4 eV. However there is always some arbitrariness to the energy positions of calculated spectra and this proximity does not by itself guarantee good agreement between the experimental and calculated spectra. What makes the agreement excellent is that the relative positions of the main features of the experimental spectrum align perfectly with those of the calculation when the latter photon energy scale is multiplied by 1.24 and shifted accordingly. The relative intensities of the calculated peaks also follow the experimental intensities reasonably well.

4 Conclusions

We have reported the experimental O K-edge NEXAFS spectrum for the first time for clean BaO. The first pre-edge peak for BaO is at 531.2 eV, which is ~2.5 eV lower than what was reported earlier in the literature. The spectrum matches very well with the latest calculations in the literature. We have also reported the O K-edge NEXAFS spectrum for $Ba(OH)_2$ and the O and N K-edge spectra for $Ba(NO_3)_2$ for the first time. Controlled preparation of $BaCO_3$ shows that the spectra reported earlier in the literature for BaO actually correspond to $BaCO_3$, and these previous measurements apparently suffered heavily from CO_2 contamination. Optimization of the preparation protocols for Ba compounds was facilitated by the use of APXPS, which provided in situ monitoring of chemical composition and measurement of spectra in gas environment.

5 Acknowledgements

We acknowledge support by the Director, Office of Science, Office of Basic Energy Sciences, and by the Division of Chemical Sciences, Geosciences and Biosciences of the US Department of Energy at LBNL under Contract No. DE-AC02-05CH11231.

6 References

Bandis, C., et al. (1999). "Photoelectron emission studies of cleaved and excimer laser irradiated single-crystal surfaces of NaNO3 and NaNO2." Surface Science **442**(3): 413-419, DOI: 10.1016/S0039-6028(99)00953-X

Bluhm, H., et al. (2006). "Soft X-ray microscopy and spectroscopy at the molecular environmental science beamline at the Advanced Light Source." Journal of Electron Spectroscopy and Related Phenomena **150**(2-3): 86-104, DOI: 10.1016/j.elspec.2005.07.005

Boffito, C. (2000). Barium. Kirk-Othmer Encyclopedia of Chemical Technology, John Wiley & Sons, Inc.

Carrier, X., et al. (1999). "Reaction of CO2 with MgO(100) surfaces." Surface Review and Letters **6**(6): 1237-1245, DOI: 10.1142/S0218625x99001396

Cooper, H. S. (1929) Patent: "Process of producing high vacua", US1721544 A, Kemet Lab Company Inc

Doyle, C. S., et al. (1999). "The interaction of carbon dioxide with single crystal CaO(100) surfaces." Surface Review and Letters **6**(6): 1247-1254, DOI: 10.1142/S0218625x99001403

Finch, A. A., et al. (2010). "Ba XAFS in Ba-rich standard minerals and the potential for determining Ba structural state in calcium carbonate." Chemical Geology **270**(1-4): 179-185, DOI: 10.1016/j.chemgeo.2009.11.015

Garvie, L. A. J., et al. (1994). "Use of Electron-Energy-Loss near-Edge Fine-Structure in the Study of Minerals." American Mineralogist **79**(5-6): 411-425,

Kim, D. H., et al. (2008). "Roles of Pt and BaO in the sulfation of Pt/BaO/Al2O3 lean NOx trap materials: Sulfur K-edge XANES and Pt L-III XAFS studies." Journal of Physical Chemistry C **112**(8): 2981-2987, DOI: 10.1021/jp077563i

Kim, D. H., et al. (2006). "Effect of barium loading on the desulfation of Pt-BaO/Al2O3 studied by H-2 TPRX, TEM, sulfur K-edge XANES, and in situ TR-XRD." Journal of Physical Chemistry B **110**(21): 10441-10448, DOI: 10.1021/jp060119f

Kim, D. H., et al. (2009). "Effects of Sulfation Level on the Desulfation Behavior of Presulfated Pt-BaO/Al2O3 Lean NOx Trap Catalysts: A Combined H-2 Temperature-Programmed Reaction, in Situ Sulfur K-Edge X-ray Absorption Near-Edge Spectroscopy, X-ray Photoelectron Spectroscopy, and Time-Resolved X-ray Diffraction Study." Journal of Physical Chemistry C **113**(17): 7336-7341, DOI: 10.1021/jp900304h

Lederer, E. A. (1934) Patent: "Means for producing high vacuum", US1952717 A, Rca Corp

Li, Y., et al. (2012). "Characterization of the Double Perovskite Ba2BixSc0.2Co1.8-xO6-delta (x=0.1, 0.2)." Chemistry of Materials **24**(21): 4114-4122, DOI: 10.1021/cm3021484

McEwen, K. L. (1961). "Electronic Structures and Spectra of Some Nitrogen-Oxygen Compounds." Journal of Chemical Physics **34**(2): 547-555, DOI: 10.1063/1.1700981

McLeod, J. A., et al. (2010). "Band gaps and electronic structure of alkaline-earth and post-transition-metal oxides." Physical Review B **81**(24), DOI: 10.1103/PhysRevB.81.245123

Miller, R. C., et al. (1963). "Quantitative Studies of Optical Harmonic Generation in CdS, BaTiO3, and KH2PO4 Type Crystals." Physical Review Letters **11**(4): 146-149, DOI: 10.1103/PhysRevLett.11.146

Mudiyanselage, K., et al. (2009). "Reactivity of a thick BaO film supported on Pt(111): adsorption and reaction of NO2, H2O, and CO2." Langmuir **25**(18): 10820-10828, DOI: 10.1021/la901371g

Nakai, S.-i., et al. (1987). "OxygenKx-ray-absorption near-edge structure of alkaline-earth-metal and 3d-transition-metal oxides." Physical Review B **36**(17): 9241-9246, DOI: 10.1103/PhysRevB.36.9241

Ogletree, D. F., et al. (2009). "Photoelectron spectroscopy under ambient pressure and temperature conditions." Nuclear Instruments & Methods in Physics Research Section a-Accelerators Spectrometers Detectors and Associated Equipment **601**(1-2): 151-160, DOI: 10.1016/j.nima.2008.12.155

Protheroe, A. R., et al. (1983). "The Electron-Energy Loss Spectra of Some Alkaline-Earth Oxides." Surface Science **126**(1-3): 534-542, DOI: 10.1016/0039-6028(83)90754-9

Ricken, D. E., et al. (1991). "A Photoemission-Study of the Surface Carbonate Species on Ag(110)." Journal of Chemical Physics **94**(12): 8592-8599, DOI: 10.1063/1.460041

Rodriguez, J. A. (1990). "The Adsorption of Nitrogen Dioxide, Nitrate and Sulfate on Ag(110) - A Quantum-Chemical Study." Surface Science **230**(1-3): 335-349, DOI: 10.1016/0039-6028(90)90043-8

Rodriguez, J. A., et al. (2000). "Reaction of NO2 with Zn and ZnO: Photoemission, XANES, and density functional studies on the formation of NO3." Journal of Physical Chemistry B **104**(2): 319-328, DOI: 10.1021/jp993224g

Rodriguez, J. A., et al. (2001). "Chemistry of NO2 on oxide surfaces: Formation of NO3 on TiO2(110) and NO2 <-> O vacancy interactions." Journal of the American Chemical Society **123**(39): 9597-9605, DOI: 10.1021/ja011131i

Rodriguez, J. A., et al. (2000). "Chemistry of NO2 on CeO2 and MgO: Experimental and theoretical studies on the formation of NO3." Journal of Chemical Physics **112**(22): 9929-9939, DOI: 10.1063/1.481629

Schmitz, P. J. and R. J. Baird (2002). "NO and NO2 adsorption on barium oxide: Model study of the trapping stage of NOx conversion via lean NOx traps." Journal of Physical Chemistry B **106**(16): 4172-4180, DOI: 10.1021/jp0133992

Takahashi, N., et al. (1996). "The new concept 3-way catalyst for automotive lean-burn engine: NOx storage and reduction catalyst." Catalysis Today **27**(1-2): 63-69, DOI: 10.1016/0920-5861(95)00173-5

Tsami, A., et al. (2006). "Model NSR catalysts: Fabrication and reactivity of barium oxide layers on Cu(111)." Surface Science **600**(17): 3403-3418, DOI: 10.1016/j.susc.2006.06.029

Verhoeven, J. A. T. and H. Van Doveren (1980). "XPS Studies on Ba, BaO and the Oxidation of Ba." Applied Surface Science **5**(4): 361-373, DOI: 10.1016/0378-5963(80)90101-4

Verhoeven, J. A. T. and H. Van Doveren (1982). "Interactions of Residual Gases with a Barium Getter Film as Measured by AES and XPS." Journal of Vacuum Science & Technology **20**(1): 64-74, DOI: 10.1116/1.571310

Wu, M. K., et al. (1987). "Superconductivity at 93-K in a New Mixed-Phase Y-Ba-Cu-O Compound System at Ambient Pressure." Physical Review Letters **58**(9): 908-910, DOI: 10.1103/PhysRevLett.58.908

Yamashita, H. and R. Kato (1970). "Vacuum Ultraviolet Absorption in Alkali-Nitrites and Alkali-Nitrates." Journal of the Physical Society of Japan **29**(6): 1557-1561, DOI: 10.1143/Jpsj.29.1557

Yang, L., et al. (2011). "Promotion of water-mediated carbon removal by nanostructured barium oxide/nickel interfaces in solid oxide fuel cells." Nature Communications **2**, DOI: 10.1038/ncomms1359

Zhou, D., et al. (2008). "Assignment of Polarization-Dependent Peaks in Carbon K-Edge Spectra from Biogenic and Geologic Aragonite." Journal of Physical Chemistry B **112**(41): 13128-13135, DOI: 10.1021/jp803176z